Annealing of the divacancy-oxygen and vacancy-oxygen complexes in silicon

M. Mikelsen, J. H. Bleka, J. S. Christensen, E. V. Monakhov, and B. G. Svensson
Department of Physics, Physical Electronics, University of Oslo, P.O. Box 1048, Blindern, N-0316 Oslo, Norway

J. Härkönen
Helsinki Institute of Physics, P.O. Box 64, FIN-00014, University of Helsinki, Finland

B. S. Avset*
SINTEF ICT, P.O. Box 124, Blindern, N-0314 Oslo, Norway

(Received 18 December 2006; revised manuscript received 1 February 2007; published 9 April 2007)

After low dose electron irradiation, annealing kinetics of divacancy-oxygen (V_2O) and vacancy-oxygen (VO) complexes in carbon-lean *n*-type magnetic Czochralski (MCZ) and diffusion-oxygenated float-zone (DOFZ) Si samples has been studied in detail. The samples were of *n* type with a phosphorus doping concentration in the 10^{12} cm^{-3} range, and the analysis was conducted by means of deep-level transient spectroscopy (DLTS). An exponential decrease in the V_2O concentration with time during isothermal annealing at temperatures in the range 275–355 °C has been observed. The activation energy for the V_2O annealing is found to be 2.02 ± 0.12 eV, with a preexponential factor in the 10^{13} s^{-1} range, which strongly suggests that dissociation of V_2O is the dominating mechanism. The binding energy of the vacancy to the V_2O complex has been estimated as ~1.7 eV. An increase in the VO concentration is observed in the initial phase of the V_2O annealing, which is supportive of V_2O dissociation through the reaction $V_2O \rightarrow VO+V$. After the initial increase, a close to first order decrease in the VO concentration is observed, consistent with that VO mainly anneals by migration and trapping at oxygen interstitial sites, similarly to what has been reported in previous high-dose studies using infrared spectroscopy. The vacancy-oxygen-hydrogen complex (VOH) is formed after long time annealing. The formation of VOH is followed by a decrease at the same rate as VO, and it is suggested that VOH dissociates ($VOH \rightarrow VO+H$). The experimental data have been compared with kinetic simulations and show good agreement with a model where the main processes are dissociation of VO and V_2O, migration and subsequent trapping of VO ultimately giving rise to the electrically inactive vacancy-dioxygen pair (VO_2) and interactions involving atomic hydrogen.

DOI: 10.1103/PhysRevB.75.155202 PACS number(s): 71.55.−i, 61.80.Fe

I. INTRODUCTION

Oxygen is one of the most common and important impurities in silicon, and is mainly present in the form of an electrically inactive interstitial configuration (O_i). It is, therefore, important to understand the behavior of oxygen-related complexes, and one of the most fundamental of these is the divacancy-oxygen complex (V_2O). Irradiation at room temperature of silicon with a sufficient oxygen concentration is known to produce O related defects since O_i is an effective trap for mobile vacancies. Initially, at low radiation doses, vacancy-oxygen (VO) complexes are formed.[1,2] As the dose increases, VO can capture another vacancy forming V_2O.[3] V_2O can also be formed when O_i traps migrating divacancies at elevated temperatures.[4–7] Despite the fundamental nature of V_2O, the positions of its electrical levels in the band gap have not been established until recently.[5–8]

The experimental identification of V_2O was made in an electron paramagnetic resonance (EPR) study by Lee and Corbett.[3] The defect was found to be present with an intensity similar to that of the divacancy (V_2) in high-dose electron-irradiated (5×10^{18} cm^{-2}) Czochralski (CZ) Si. It was found that V_2O disappeared after annealing at 350 °C, and it was speculated that V_2O either acts as a sink for migrating vacancies giving rise to V_3O or is lost via interaction with O_i, forming V_2O_2. In a positron annihilation spectroscopy study on Cz-Si irradiated by electrons with a lower dose of 1×10^{18} cm^{-2}, no considerable concentration of V_2O was observed in as-irradiated samples.[4] It was found, however, that V_2O could be formed when V_2 annealed. It was proposed that V_2O was formed as a result of divacancy migration and subsequent trapping at an O_i site ($V_2+O_i \rightarrow V_2O$). A similar conclusion has also been reached in low dose studies of high resistivity silicon using deep-level transient spectroscopy (DLTS).[5,7] In Ref. 4, the positron trap assigned to V_2O was found to decrease in concentration at ~400 °C, simultaneously as two other traps emerged. The activation energy for the annealing of the trap attributed to V_2O was estimated to 2.1 eV and mechanisms such as dissociation, trapping during migration ($V_2O+O_i \rightarrow V_2O_2$) and capturing of released vacancies ($V_2O+V \rightarrow V_3O$) were discussed. For further progress, detailed studies of the annealing kinetics of V_2O and associated multivacancy-oxygen complexes are required using electrical and optical techniques. Such studies are, however, scarce in the literature and this is in part due to the fact that V_2O has a Si-O-Si bonding structure that is very similar to that of VO. Techniques such as infrared (IR) spectroscopy, which can be used to determine the local vibrational modes and electronic transitions of defects, cannot easily distinguish the V_2O absorption band from the dominating VO band: calculations based on density functional theory have predicted that the absorption band of

these two defects are very close in position.[9] In a low-temperature IR absorption study on irradiated silicon an absorption band at 833 cm^{-1} was ascribed to V_2O.[10] This band did, however, appear only as a shoulder at the low energy tail of the much more intense VO absorption band located at 836 cm^{-1}.

Furthermore, despite the early EPR observations, the electrical activity of V_2O was established only recently. In a series of DLTS studies it was shown that V_2O can be formed in irradiated diffusion-oxygenated float-zone (DOFZ) Si via annealing of V_2.[5,7] The electrical properties of V_2O are similar to those of V_2, with a (0/+) donor level at $\sim E_v+0.24$ eV,[11] a (−/0) acceptor level at $\sim E_c-0.47$ eV and a (=/−) acceptor level at $\sim E_c-0.23$ eV,[5] where E_v and E_c are the energies of the edges of the valence- and conduction-band, respectively. It has also been shown that the transition from V_2 to V_2O can occur in Cz-Si with mechanically polished surfaces, minimizing the exposure to hydrogen during the sample preparation.[8]

Other DLTS studies on Cz-Si and FZ-Si did not reveal any levels related V_2O, neither directly after irradiation nor after V_2 annealing.[12] However, DLTS is applicable to very low concentrations of defects, contrary to EPR, IR, and positron-annihilation spectroscopy. The mechanism for V_2 annealing in DLTS studies may therefore be sensitive to the presence of impurities with a relatively low concentration. It has been shown that H affects considerably the annealing of V_2, effectively preventing formation of V_2O.[13] Hence, one can speculate that the annealing of V_2 in Ref. 12 may be caused by interaction with residual hydrogen.

In this work, we have performed a detailed DLTS study on the annealing of V_2O and VO, using two different kinds of electron-irradiated Si materials; high purity DOFZ-Si and carbon-lean magnetic Czochralski (MCZ) Si. Isothermal annealing has been carried out at different temperatures in the range 275–355 °C. The annealing of V_2O follows first-order kinetics and suggests that dissociation is the dominant annealing mechanism with minor (if any) formation of higher order multivacancy-oxygen complexes. The loss of VO displays a more complex behavior than V_2O, and invokes several mechanisms such as migration, trapping by O_i, dissociation, and interaction with residual hydrogen impurities. The annealing of VO and V_2O is modeled, applying the theory of diffusion limited reactions.[14] The results of the simulation agree well with those of the experiments.

II. EXPERIMENT

Two sets of samples were studied: the first set was prepared from n^- MCZ-Si and the second set was prepared from n^- DOFZ-Si, see Table I for doping concentrations. The preparation of the second material includes a step where high purity FZ-Si is oxygen enriched: the FZ-wafers are dry oxidized for 21 h at 1200 °C, and a subsequent anneal is then performed at 1200 °C in a N_2 atmosphere where O atoms from the preformed SiO_2 surface layer diffuse into the bulk Si. For all samples boron and phosphorus implantations with post-implant annealing were performed in order to form p^+-n^--n^+ diodes. As a final step aluminum contacts were deposited. Secondary-ion mass spectrometry (SIMS) has been used to determine the oxygen and carbon concentrations. A survey of the samples is found in Table I. All of the samples were irradiated with 6 MeV electrons at room temperature to doses in the range $2-4\times10^{12}$ cm^{-2}.

TABLE I. Survey of the samples used in the study.

Sample	Doping concentration (cm^{-3})	Carbon concentration (cm^{-3})	Oxygen concentration (cm^{-3})
MCZ-Si	5.5×10^{12}	$\leqslant10^{16}$	$(5-10)\times10^{17}$
DOFZ-Si	5.0×10^{12}	$(2-4)\times10^{16}$	$(2-3)\times10^{17}$

The DLTS measurements were performed using two setups. One is based on a Booton 7200 capacitance meter, and the other on a HP 4280A capacitance meter described elsewhere.[15] The temperature of the sample was scanned between 77 K and 300 K, and in some cases between 12 K and 300 K. The measured capacitance transients were averaged in intervals of 1 K. The DLTS signal was extracted by using a lock-in type weighting function, and different spectra were obtained corresponding to six rate windows ranging from $(20\ ms)^{-1}$ to $(640\ ms)^{-1}$.

After irradiation the samples were preannealed in two steps. The first step involved annealing for 15 min at 225 °C, in order to remove minor, unstable defects that overlap with V_2 in the DLTS spectrum. The second step consisted of extended annealing at 255 or 300 °C in order to ensure a transition from V_2 to V_2O.[7] One sample was also annealed for 70 h at 205 °C before this annealing step. An overview of the annealing history for each sample can be found in Table II.

Isothermal annealing treatment was then performed at temperatures in the range 275–355 °C. This annealing temperature always exceeded the temperatures used in the pretreatment. DLTS measurements were conducted before and after each annealing step.

III. RESULTS

Three dominant DLTS peaks at $\sim E_c-0.18$, $E_c-0.23$, and $E_c-0.43$ eV are present after irradiation. These are identified as the vacancy-oxygen pair, VO, the doubly negative divacancy, $V_2(=/-)$, and the singly negative divacancy, $V_2(-/0)$, respectively. After annealing for 15 min at 225 °C, some minor defects overlapping with $V_2(-/0)$ are annealed out, resulting in relatively pure V_2 peaks with a close one-to-one relation between the amplitudes of the $E_c-0.23$ and $E_c-0.43$ eV levels. In the second step of the preannealing the expected transition from V_2 to V_2O takes place in both the DOFZ- and MCZ-Si samples [Fig. 1(a)] and the corresponding levels appear at $E_c-0.23$ and $E_c-0.47$ eV.

A minor peak forms at ~157 K in the $(640\ ms)^{-1}$ spectrum during the V_2 to V_2O transition [Fig. 1(a)]. This peak is present in all the samples. The formation kinetics and identity of this level is discussed elsewhere.[16] The 157 K peak is slightly broader in the MCZ-Si than in the DOFZ-Si samples

TABLE II. Annealing history of the samples used in the study.

Sample number	Type	Preannealing treatment	Annealing temperature (isothermal)
A	MCZ	15 min at 225 °C 15 min at 300 °C	355 °C
B	MCZ	15 min at 225 °C 15 min at 300 °C	335 °C
C	MCZ	15 min at 225 °C 15 min at 300 °C	325 °C
D	MCZ	15 min at 225 °C 15 min at 300 °C	315 °C
E	MCZ	15 min at 225 °C 15 min at 300 °C	305 °C
F	MCZ	15 min at 225 °C 360 min at 255 °C	290 °C
G	MCZ	15 min at 225 °C 360 min at 255 °C	275 °C
H	DOFZ	15 min at 225 °C 15 min at 300 °C	355 °C
I	DOFZ	15 min at 225 °C 15 min at 300 °C	350 °C
J	DOFZ	15 min at 225 °C 15 min at 300 °C	335 °C
K	DOFZ	15 min at 225 °C 70 h at 205 °C 15 min at 300 °C	325 °C
L	DOFZ	15 min at 225 °C 360 min at 255 °C	290 °C
M	DOFZ	15 min at 225 °C 360 min at 255 °C	275 °C

[Fig. 1(b)], and improving the energy resolution of the DLTS spectra using a weighting function described in Ref. 17, it is observed that the broadening in MCZ-Si samples is caused by an additional minor peak at ~150 K.

During isothermal annealing in the temperature range 275 to 355 °C, the intensity of the two V_2O peaks decrease [Figs. 1(a) and 1(b)]. After prolonged annealing, [250 min at 325 °C, Fig. 1(b)], the amplitude of the doubly negative peak, $V_2O(=/-)$, reaches the background level. However, a peak still remains at the position of $V_2O(-/0)$. This observation supports a suggestion made previously, that a minor

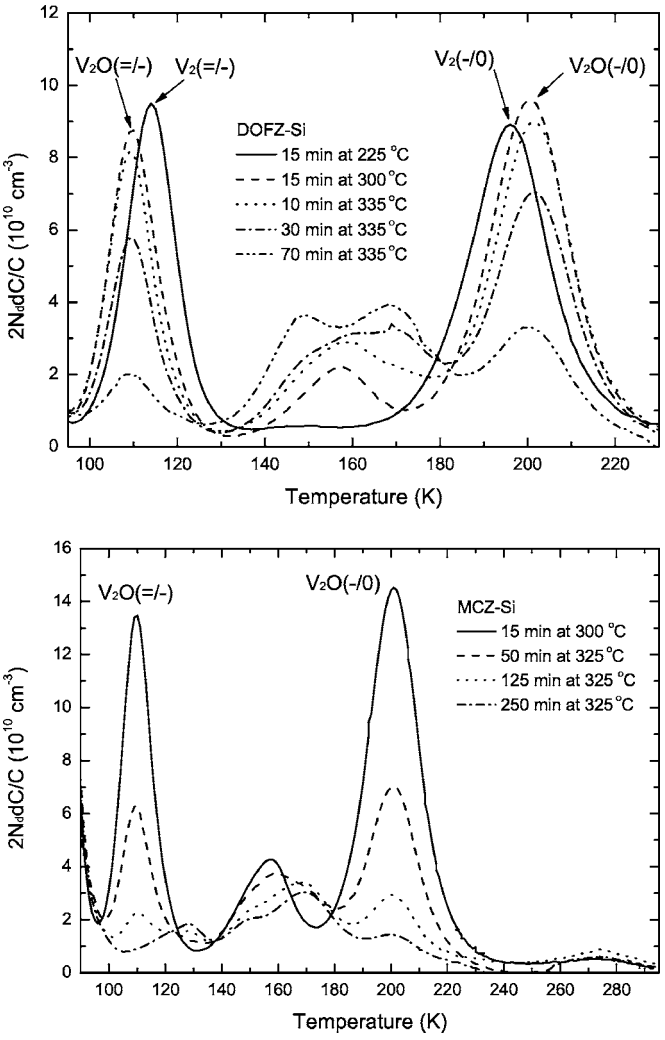

FIG. 1. DLTS spectra of irradiated DOFZ-Si (a) and MCZ-Si (b) samples after annealing.

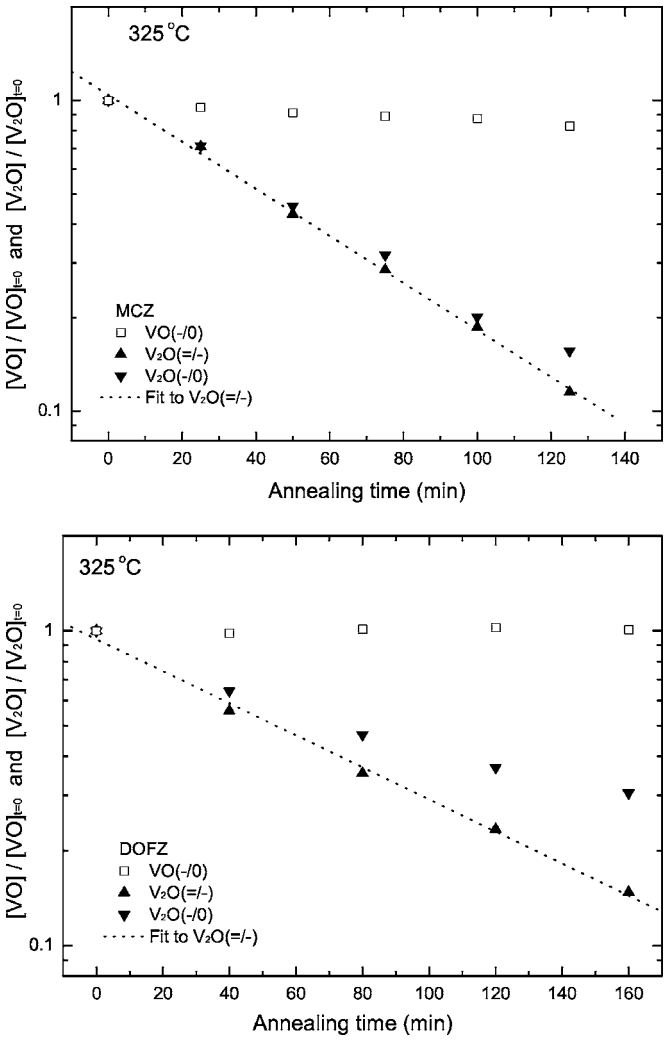

FIG. 2. Normalized intensities of $V_2O(-/0)$, $V_2O(=/-)$ and VO with respect to those at $t=0$ versus annealing time during isothermal annealing at 325 °C for MCZ-Si (a) and DOFZ-Si (b) samples. The dotted line represents an exponential decay fit [Eq. (1)] to $V_2O(=/-)$.

peak forms at this position during the V_2 to V_2O transition,[7] and it appears to grow somewhat further during the loss of V_2O in the DOFZ samples.

In the temperature interval between the two V_2O peaks several minor overlapping levels occur, and the DLTS spectra in this region can be fit with a sum of single peaks. The fitting is done by a computer program that explores an array of different possible combinations of single peaks, applied to all six rate windows, and returns the best fit.[18] It is possible to estimate the activation enthalpy and apparent capture cross sections, although, the accuracy of these values are limited. The fitting reveals the presence of three peaks in this region. One of these is the ~157 K level discussed previously, which decreases gradually in intensity after annealing. There is also a level at ~170 K, with an estimated activation enthalpy of ~0.31 eV and an apparent capture cross section of 4×10^{-17} cm^2. This level has a larger intensity in the DOFZ-Si samples than in the MCZ-Si samples. This also holds for a third level at ~148 K, which has an estimated

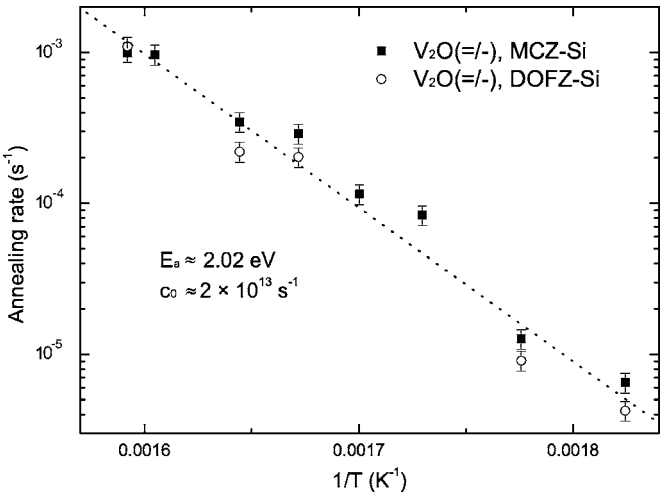

FIG. 3. Arrhenius plot for the annealing rates of $V_2(=/-)$ in MCZ- and DOFZ-Si. The dotted line is an exponential fit to all the data from both the DOFZ- and MCZ-Si samples. The error bars indicate an experimental error of 15%.

activation enthalpy of ~0.27 eV and an apparent capture cross section of 5×10^{-17} cm^2. The appearance of this third level depends on how the pretreatment was performed: in a DOFZ-Si sample that was pretreated for 70 h at 205 °C, this level does not form after subsequent annealing at 325 °C.

In the MCZ-samples a level is also observed at ~280 K, Fig. 1(b). This level has been reported previously,[18] and is located close to the middle of the band gap, with an activation enthalpy of 0.58 eV below E_c and an apparent capture cross section of 4×10^{-16} cm^2. Finally, a minor level at ~50 K, 0.10 eV below E_c, is revealed in DOFZ-Si (not shown), and it remains stable during the V_2O annealing.

In the following we will mainly focus on the VO and V_2O peaks, which dominate the spectra. The concentration of $V_2O(=/-)$ exhibits a exponential decrease with time:

$$[V_2O](t) = [V_2O](t=0)\exp[-c(T)t], \tag{1}$$

where $[V_2O]$ denotes the concentration of V_2O and $c(T)$ is a temperature dependent rate constant. This relation holds for all annealing temperatures in both DOFZ- and MCZ-Si. As an example, the normalized concentration is plotted versus annealing time at 325 °C for MCZ- and DOFZ-Si in Figs. 2(a) and 2(b), respectively. The amplitude of $V_2O(-/0)$ is consistently higher than for $V_2O(=/-)$, which is caused by the minor level overlapping with $V_2O(-/0)$.

In Fig. 3, the rate constant, $c(T)$, for $V_2O(=/-)$ is depicted versus the inverse absolute temperature. For a singly activated process, an Arrhenius behavior is expected;

$$c(T) = c_0 \exp(-E_a/kT), \tag{2}$$

where E_a is the activation energy and c_0 is the prefactor. For both MCZ- and DOFZ-Si $c(T)$ obeys an Arrhenius behavior with some scatter. By fitting all the data for both types of samples with a straight line, an activation energy of 2.02 ± 0.12 eV is obtained. The prefactor is determined to 2×10^{13} s^{-1}, with about one order of magnitude in uncertainty.

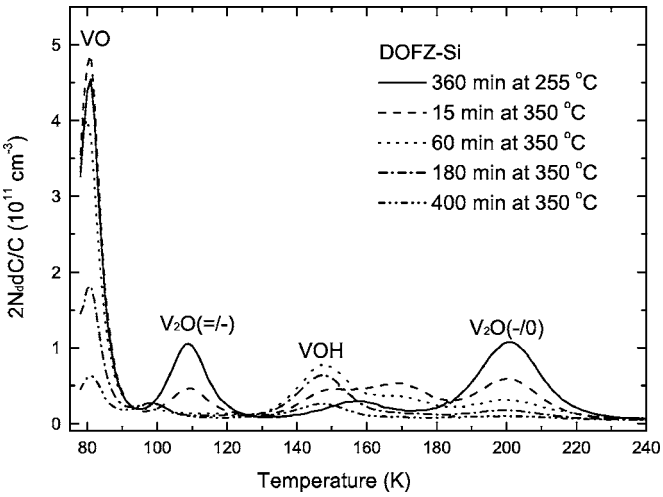

FIG. 4. DLTS spectra of DOFZ-Si after annealing for prolonged duration at 350 °C.

In parallel to the annealing of V_2O a slight increase in the VO concentration is observed in the DOFZ-Si samples, while the opposite holds for the MCZ-Si samples. In order to study the annealing behavior of VO more closely, a DOFZ-Si sample was subjected to heat treatment at 350 °C for extended periods of time. The initial increase in the VO concentration is followed by a decrease after longer annealing times (Fig. 4). Ultimately, this decrease approaches an exponential decay, as illustrated in Fig. 5 where the concentrations of VO and V_2O are depicted versus annealing time at 350 °C. Figure 4 also reveals the appearance of VOH(−/0), which is located 0.32 eV below E_c,[12,19–22] after sufficiently long times. Initially, the concentration of VOH increases, but is later followed by a decrease which also approaches an exponential decay, with a rate similar to that of VO, Fig. 5.

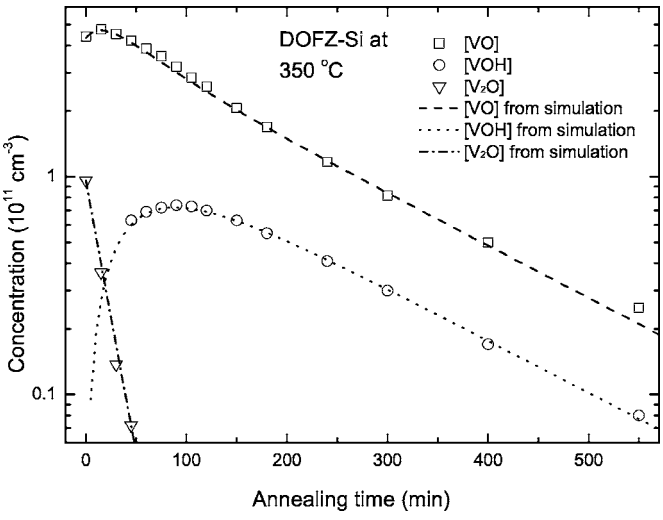

FIG. 5. Comparison between simulated and experimental concentrations of VO, VOH, and V_2O in a DOFZ-Si sample versus time during isothermal annealing at 350 °C. The dotted lines are the simulation results.

IV. DISCUSSION

For a dissociative process first order annealing kinetics and a prefactor in the range of 10^{12}–10^{13} s^{-1} is expected.[23] Both these features characterize the annealing V_2O, suggesting strongly that the complex dissociates. V_2O migration and subsequent trapping at oxygen interstitial sites, similar to the annealing process for V_2, is not likely to be a main annealing mechanism. In addition to the magnitude of the prefactor, two other arguments against migration and trapping can be put forward. The first one is that the O_i concentration is higher in MCZ-Si than in DOFZ-Si, which would result in a substantially faster annealing of V_2O in MCZ-Si than in DOFZ-Si, but this does not agree with the experimental data. The second reason is that migration and trapping would result in the formation of V_2O_2, which is believed to be electrically active with two acceptor centers similar to V_2 and V_2O.[24] No such levels have been observed. For dissociation of V_2O, two possible dissociation reactions can be considered: $V_2O \rightarrow VO+V$ and $V_2O \rightarrow V_2+O_i$. However, calculations employing density functional theory have predicted a dissociation barrier of 1.5–1.6 eV for the first reaction while the other reaction has a barrier of 2.6 eV.[24] The first reaction is, therefore, likely to dominate, and this reaction will contribute to an increase in the VO concentration consistent with the results for the DOFZ-Si samples. However, VO is not very stable at temperatures above 300 °C, and infrared spectroscopy studies have identified at least two different annealing mechanisms.[25,26] It was found that VO is mobile above 300 °C, and can anneal by migration and trapping at oxygen-interstitial sites, forming the electrically inactive VO_2 complex ($VO+O_i \rightarrow VO_2$). The rate of this process increases linearly with the O_i concentration and is presumably a major reason for the lack of increase in VO concentration in the MCZ-Si samples when V_2O starts to break up. Furthermore, dissociation of VO is also known to occur ($VO \rightarrow V+O_i$). However, in a material where oxygen is the dominant impurity, most of the monovacancies will be retrapped at an O_i site, yielding a substantial reforming of VO.

In order to reach a more quantitative understanding of the role of the various defect reactions, a kinetic model for the annealing process has been developed. In the model, dissociation of VO and V_2O and migration and trapping of VO are assumed. Further, the appearance of VOH in the DLTS spectra (Fig. 4) reveals the presence of hydrogen. VOH occurs after quite long annealing times, and at relatively low concentrations, suggesting a rather limited supply of hydrogen. Since hydrogen is expected to be highly mobile in the studied temperature range, the formation of VOH is presumably controlled by the release of trapped hydrogen. In the model, a complex XH is introduced where X denotes a trapping site for H; at elevated temperatures XH breaks up ($XH \rightarrow X+H$) and provides migrating hydrogen atoms. Several studies have reported that complexes can release H in such a way, and activation energies for trap-limited release are reported to be in the range 1.1–1.5 eV.[27–29] The released hydrogen atoms will migrate and bond to VO, forming VOH. VOH can subsequently capture a second H atom forming the electrically inactive VOH_2.[12] After an initial increase in the

TABLE III. Rate equations derived from Eqs. (3)–(13). Numerical values for the constants are given in Table IV.

Defect species	Rate equation
V_2O	$\frac{d[V_2O]}{dt} = -C_{V2O}^{Diss}[V_2O] + 4\pi R D_V[V][VO] - 4\pi R D_H[H][V_2O]$
VO	$\frac{d[VO]}{dt} = C_{V2O}^{Diss}[V_2O] + 4\pi R D_V[V][O_i] - 4\pi R D_{VO}[VO][O_i] - C_{VO}^{Diss}[VO] - 4\pi R D_V[V][VO] - 4\pi R D_H[H][VO]$
VO_2	$\frac{d[VO_2]}{dt} = 4\pi R D_{VO}[VO][O_i]$
O_i	$\frac{d[O_i]}{dt} = C_{VO}^{Diss}[VO] - 4\pi R D_{VO}[VO][O_i] - 4\pi R D_V[V][O_i]$
V	$\frac{d[V]}{dt} = C_{V_2O}^{Diss}[V_2O] - 4\pi R D_V[V][O_i] + C_{VO}^{Diss}[VO] - 4\pi R D_V[V][VO]$
VOH	$\frac{d[VOH]}{dt} = 4\pi R D_H[H][VO] - 4\pi R D_H[H][VOH] - C_{VOH}^{Diss}[VOH]$
H	$\frac{d[H]}{dt} = C_{HX}^{Diss}[HX] - 4\pi R D_H[H][X] - 4\pi R D_H[H][VO] - 4\pi R D_H[H][VOH] - 4\pi R D_H[H][V_2O]$
VOH_2	$\frac{d[VOH_2]}{dt} = 4\pi R D_H[H][VOH]$
HX	$\frac{d[HX]}{dt} = -C_{HX}^{Diss}[HX] + 4\pi R D_H[H][X]$
X	$\frac{d[X]}{dt} = C_{HX}^{Diss}[HX] - 4\pi R D_H[H][X]$

VOH concentration, a decrease with annealing time is observed (Fig. 4). The rate of this decrease is, however, too high to be explained by reactions with hydrogen only. In fact, the annealing rates of VOH and VO approach almost exactly the same value after sufficiently long times. This can be explained by dissociation of VOH through the reaction $VOH \rightarrow VO + H$. A substantial amount of VOH will reform as released H atoms again are trapped at VO complexes during migration, and the rate of this process is proportional to the concentration of VO. Since the VO concentration decreases with time, so does the rate of VOH reformation, and the annealing rate for VOH becomes essentially the same as for VO. Trapping of hydrogen by V_2O, resulting in V_2OH, is also taken into account in the model. It has, however, only a minor effect since the reaction rate between V_2O and H is expected to be of the same magnitude as that for VO and H, assuming similar capture radii, which is much lower than the dissociation rate for V_2O.

On the basis of the considerations discussed above, the following reactions have been included in the simulation

$$V_2O \rightarrow VO + V, \tag{3}$$

$$V + VO \rightarrow V_2O, \tag{4}$$

$$VO \rightarrow V + O_i, \tag{5}$$

$$V + O_i \rightarrow VO, \tag{6}$$

$$VO + O_i \rightarrow VO_2, \tag{7}$$

$$XH \rightarrow X + H, \tag{8}$$

$$X + H \rightarrow XH, \tag{9}$$

$$VOH \rightarrow VO + H, \tag{10}$$

$$VO + H \rightarrow VOH, \tag{11}$$

$$VOH + H \rightarrow VOH_2, \tag{12}$$

$$V_2O + H \rightarrow V_2OH. \tag{13}$$

The corresponding coupled differential equations can be derived by applying the theory for diffusion limited reactions developed by Waite[14] and they are given in Table III. The rate equations are solved numerically, and a survey of the values used for the various constants and boundary conditions is given in Table IV.

TABLE IV. Numerical values for the constants used in the simulation.

Constant	Explanation	Value	Comment
R	Capture radius	5 Å	
$C_{V_2O}^{Diss}$	Dissociation rate for V_2O.	$c(T)$ for V_2O, see Eq. (2). E_a=2.02 eV $c_0=2\times10^{13}$ s^{-1}	The annealing rate of V_2O, $c(T)$, found in this study. (Fig. 3)
C_{VO}^{Diss}	Dissociation rate for VO.	5.5×10^{-4} s^{-1} at 350 °C, with E_a=2.51 eV	Values taken from Ref. 25
C_{HX}^{Diss}	Dissociation rate for HX.	$C_{HX}^{Diss}=c_0\exp(-E_a/kT)$ where E_a=2.11 eV and $c_0=1\times10^{13}$ s^{-1}	Free parameter, determined by fitting of the VOH annealing curve with c_0 typical for dissociation. The accuracy is within 50%.
C_{VOH}^{Diss}	Dissociation rate for VOH.	$C_{HX}^{Diss}=0.6\times C_{VO}^{Diss}$	Free parameter, determined by fitting of the VOH annealing curve. The accuracy is within 50%.
D_{VO}.	Diffusivity of VO.	5.0×10^{-16} cm^2 s^{-1} at 350 °C, with E_a=2.06 eV	Values taken from Ref. 25, but increased by 25%.
D_V, D_H	Diffusivities of V and H.	$D_V=D_H=10^4\times D_{VO}$	Assumed to be very high.
$[HX]_{t=0}$	Initial concentration of HX.	1×10^{13} cm^{-3}	Free parameter determined by fitting of the VOH annealing curve. The accuracy is 1–2 orders of magnitude with $\sim10^{13}$ cm^{-3} as a lower limit.
$[V_2O]_{t=0}$ $[VO]_{t=0}$	Initial concentrations of V_2O and VO.	Measured	
$[VOH]_{t=0}$ $[V]_{t=0}$ $[H]_{t=0}$ $[X]_{t=0}$	Initial concentrations of VOH, V, H, and X.	Put equal to 0.	

Figure 5 displays the result of the simulations together with the data from DOFZ-Si after annealing at 350 °C. Three parameters were free when fitting the curves to the data in Fig. 5; the initial HX concentration, $[HX]_{t=0}$, the HX dissociation rate, C_{HX}^{Diss}, and the VOH dissociation rate, C_{VOH}^{Diss}. The result of the fit is not very sensitive to $[HX]_{t=0}$, and an increase from the value given in Table IV by one order of magnitude results in no significant change of the fitting curves. Estimates of the errors in the free parameters are given in Table IV. The diffusivity prefactor for VO is increased by 25% compared to the value given in Ref. 25. Otherwise, the parameter values used are identical with those in Ref. 25 and those deduced from the current experiment. As can be seen from Fig. 5, the model is in good quantitative agreement with the experimental data for V_2O, VO as well as VOH annealing, and provides additional support for the conclusion that V_2O annealing is dominated by dissociation. Furthermore, as shown in Fig. 5, the model also accounts for the increase in VO concentration observed during V_2O annealing in DOFZ-Si. Moreover, in MCZ-Si, where the O content is higher and annealing of VO via migration to O_i is strongly promoted, no increase in the VO concentration during annealing of V_2O is predicted by the model, fully consistent with the experimental observations.

In this context, it is interesting to note that a dissociation energy of ~2.0 eV for reaction (3) implies a binding energy of ~1.7 eV. This assumes a migration energy of ~0.3 eV for V,[30] which is expected to be in the neutral charge state during annealing, and no extra reaction barrier, i.e., the dissociation energy equals the sum of the binding and migration energy for V. The value of ~1.7 eV is somewhat higher than 1.3 eV, which has been predicted by theory,[24] but of the same magnitude.

Finally, it should be pointed out that several studies, using IR absorption, DLTS and Hall-effect techniques, have reported a metastable configuration of VO_2 labeled VO_2^*,[31–33] which is considered to be electrically active with a shallow acceptor state at $E_c-0.06$ eV.[32,33] VO_2^* has a total energy that is only 0.25 eV higher than VO_2, and the equilibrium fraction of VO_2^* increases with temperature.[31] During sub-

sequent rapid cooling to room temperature, centers in the (*) configuration are frozen and do not revert back to the ground state. Indeed, after annealing for 9 h at 350 °C and then quenching to room temperature we observe a level at $\sim E_c - 0.06$ eV in the DOFZ-Si sample. The concentration of this level is ~5% of the initial VO concentration, in close agreement with that expected for VO_2^* according to the IR-data in Ref. 31 where the remaining fraction of annealed VO centers occurs as VO_2. Hence, these data provide additional evidence for reaction (7) being the dominant one for the annealing of VO in our samples.

V. SUMMARY

The annealing of V_2O is shown to exhibit first order kinetics in both MCZ and DOFZ-Si. The activation energy of the process is determined to 2.02 ± 0.12 eV, and the prefactor is $\sim 2 \times 10^{13}$ s^{-1}. The value of the prefactor strongly suggests dissociation as the main annealing mechanism for V_2O. A kinetic model is developed invoking dissociation of VO and V_2O, migration of VO and subsequent trapping at O_i sites, release of trapped hydrogen atoms and interaction of hydrogen with vacancy-type defects. Taking diffusivity and dissociation values from literature and from the current study, the model displays excellent agreement with experimental data. In particular, the simulation results represent further solid support for dissociation as the dominant annealing mechanism for V_2O. Finally, based on the experimental results, the binding energy of V to the V_2O complex is estimated as ~1.7 eV, in reasonable agreement with theoretical predictions.

ACKNOWLEDGMENTS

Financial support by the Norwegian Research Council ("Forskerprosjekt" and Strategic University Program on Advanced Sensors for Microtechnology) is gratefully acknowledged. Enlightening discussions with Leonid Murin are also highly appreciated.

*Present address: Statens Strålevern, Grini næringspark 13, P.O. Box 55, 1332 Østerås, Norway.

[1] G. D. Watkins and J. W. Corbett., Phys. Rev. **121**, 1001 (1961).
[2] J. W. Corbett, G. D. Watkins, R. M. Chrenko, and R. S. McDonald, Phys. Rev. **121**, 1015 (1961).
[3] Y. H. Lee and J. W. Corbett, Phys. Rev. B **13**, 2653 (1976).
[4] A. Kawasuso, M. Hasegawa, M. Suezawa, S. Yamaguchi, and K. Sumino, Appl. Surf. Sci. **85**, 280 (1995).
[5] E. V. Monakhov, B. S. Avset, A. Hallén and B. G. Svensson, Phys. Rev. B **65**, 233207 (2002).
[6] G. Alfieri, E. V. Monakhov, B. S. Avset, and B. G. Svensson, Phys. Rev. B **68**, 233202 (2003).
[7] M. Mikelsen, E. V. Monakhov, G. Alfieri, B. S. Avset, and B. G. Svensson, Phys. Rev. B **72**, 195207 (2005).
[8] V. P. Markevich, A. R. Peaker, S. B. Lastovskii, L. I. Murin and J. L. Lindström, J. Phys.: Condens. Matter **15**, S2779 (2003).
[9] M. Pesola, J. von Boehm, T. Mattila, and R. M. Nieminen, Phys. Rev. B **60**, 11449 (1999).
[10] J. L. Lindström, L. I. Murin, V. P. Markevich, T. Hallberg, and B. G. Svensson, Physica B **273**, 291 (1999).
[11] M.-A. Trauwaert, J. Vanhellemont, H. E. Maes, A.-M. van Bavel, G. Langouche, and P. Clauws, Appl. Phys. Lett. **66**, 3056 (1995).
[12] P. Pellegrino, P. Lévêque, J. Lalita, A. Hallén, C. Jagadish, and B. G. Svensson, Phys. Rev. B **64**, 195211 (2001).
[13] E. V. Monakhov, A. Ulyashin, G. Alfieri, A. Yu. Kuznetsov, B. S. Avset, and B. G. Svensson, Phys. Rev. B **69**, 153202 (2004).
[14] T. R. Waite, Phys. Rev. **107**, 463 (1957).
[15] B. G. Svensson, K.-H. Rydén, and B. M. S. Lewerentz, J. Appl. Phys. **66**, 1699 (1989).
[16] M. Mikelsen, E. V. Monakhov, B. S. Avset, and B. G. Svensson, Phys. Scr., T **126**, 81 (2006).
[17] P. Pellegrino, Ph.D. Thesis, Royal Institute of Technology, Stockholm (2001).
[18] J. H. Bleka, E. V. Monakhov, A. Ulyashin, F. D. Auret, A. Yu. Kuznetsov, B. S. Avset, and B. G. Svensson, Solid State Phenom. **108**, 553 (2005).
[19] K. Bonde Nielsen, L. D. Dobaczewski, K. Goscinski, R. Bendesen, O. Andersen, and B. Bech Nielsen, Physica B **273**, 167 (1999).
[20] A. R. Peaker, J. H. Evans-Freeman, L. Rubaldo, I. D. Hawkins, K. Vernon-Parry, and L. Dobaczewski, Physica B **273**, 243 (1999).
[21] Y. Tokuda and T. Seki, Semicond. Sci. Technol. **15**, 126 (2000).
[22] P. Lévêque, P. Pellegrino, A. Hallén, B. G. Svensson, and V. Privitera, Nucl. Instrum. Methods Phys. Res. B **174**, 297 (2001).
[23] J. W. Corbett, *Electron-Radiation Damage in Semiconductors and Metals*, edited by F. Seitz and D. Turnbull (Academic, New York, 1966), p. 39.
[24] J. Coutinho, R. Jones, S. Öberg, and P. R. Briddon, Physica B **340**, 523 (2003).
[25] B. G. Svensson and J. L. Lindström, Phys. Rev. B **34**, 8709 (1986).
[26] B. G. Svensson, J. L. Lindström, and J. W. Corbett, Appl. Phys. Lett. **47**, 841 (1985).
[27] Y. L. Huang, Y. Ma, R. Job, and A. Ulyashin, J. Appl. Phys. **96**, 7080 (2004).
[28] R. C. Newman, J. H. Tucker, A. R. Brown, and S. A. McQuaid, J. Appl. Phys. **70**, 3061 (1991).
[29] H. J. Stein and S. K. Hahn, J. Electrochem. Soc. **142**, 124 2 (1995).
[30] G. D. Watkins and J. W. Corbett, Phys. Rev. **138**, 543 (1965).
[31] J. L. Lindström, L. I. Murin, B. G. Svensson, V. P. Markevich, T. Hallberg, Physica B **340**, 509 (2003).
[32] L. I. Murin, J. L. Lindström, V. P. Markevich, I. F. Medvedeva, V. J. B. Torres, J. Coutinho, R. Jones, and P. R. Briddon, Solid State Phenom. **108**, 223 (2005).
[33] L. I. Murin, V. P. Markevich, I. F. Medvedeva, and L. Dobaczewski, Semiconductors **40**, 1282 (2006).